Thin Film Nanocrystalline TiO2 Electrodes: Dependence of Flat Band Potential on pH and Anion Adsorption

Thin film nanocrystalline TiO_2 electrodes: dependence of flat band potential on pH and anion adsorption

M. Minella*[1,2], V. Maurino[1], C. Minero[1], E. Pelizzetti[1]

[1] Department of Chemistry and NIS Center of Excellence, University of Torino, Via P. Giuria 5, Torino 10125, Italy http://www.environmentalchemistry.unito.it.

[2] Rockwood Italia S.p.a. Silo Division, Via Reiss Romoli,44/12, Torino Italy

* Corresponding author. Fax +39-011-6705242; E-mail: marco.minella@unito.it.

Date of Submission: 2nd October 2013
Date of Acceptance: 4th March 2014
Email Address: marco.minella@unito.it.

Abstract

Thin nanocrystalline TiO_2 films were produced on ITO conductive glass by dip-coating of a sol-gel TiO_2 precursor. The transparent films were characterized from the optical and structural point of view with UV-Vis, Spectroscopic Ellipsometry, Raman and X-ray photoelectron spectroscopies, the roughness of the coating by AFM. The changes in the electrochemical properties features of ITO/TiO_2 electrodes were evaluated in the presence of different electrolytes (KCl, Na_2SO_4 and phosphate buffer) with the aim to clarify the role of the ion adsorption on the structure of the electrical double layer. Electrochemical tests (Cyclic Voltammetry, CV, and Impedance Electrochemical Spectroscopy, EIS) showed a strong influence of the electrolyte properties on the semiconductor band edge position in the electrochemical scale and on band bending. The CV profiles recorded can be explained by considering that the interface capacity is due to the charging of surface states (e.g. Ti(IV) surface sites coordinated by oxygen atoms, ≡Ti–OH or Ti–O–Ti). The surface charge is strongly affected also by the density and nature of adsorbed ions and by dissociation of surficial OH. Of interest the fact that for the produced nanocrystalline electrodes the flat band potential, measured from the Mott-Schottky analysis of the space charge layer capacity obtained with EIS, showed a non Nernstian behavior with the pH probably caused by a change in the surface acid-

ity as a consequence of specific anion adsorption. The modulation of flat band potential with adsorbed ions is of interest for many applications, in particular for photocatalysis (change in the redox potential of photogenerated carriers) and for photovoltaic applications like DSSC (change in the photopotentials).

Keywords: titanium dioxide, flat band potential, ion adsorption, electrochemical impedance spectroscopy, nanocrystalline films

1. Introduction

The adsorption of ions on colloids and surfaces of metal oxides have been studied extensively to understand the peculiarities of the specific adsorption phenomena on these materials. Among the wide band gap semiconductors, one of the most studied is titanium dioxide (in the allotropic form of rutile or anatase) which is widely employed in different fields: the development of Advanced Oxidation Processes (AOPs) able to achieve the abatement of refractory pollutants in air[1-4] or in aqueous solution[5-11]; the production of materials with smart surface (e.g. super hydrophilic surfaces[12, 13]) and the production of second and third generation of solar cells like DSSC and for the production of solar fuels [14]. A recent peak of interest on TiO_2 was related to the use of this semiconductor in the so called Dye Sensitized Solar Cells (DSSC) [15-17] in which nanocrystalline TiO_2 is associated to high visible absorbing dyes (usually a ruthenium or osmium complex). The main limit to the use of TiO_2 in photocatalytic processes as based material in solar cells or in devices used to synthesize high energetic products (e.g. H_2 and O_2 by water photosplitting) is the low photonic efficiency. Crucial problems are i) the high recombination yield of the valence band holes and conduction band electrons photoproduced by the absorption of photons of energy exceeding that of the semiconductor band gap (for TiO_2 3.0 – 3.2 eV) and ii) the absorption of only a little portion of the solar spectra by TiO_2. To develop strategies to increase the separation of the photoproduced charged carriers avoiding their recombination favouring interfacial charge transfer, a detailed knowledge of the TiO_2/electrolyte interface is an essential starting point.

Several studies report on the effects of the adsorption of ions on the photodegradation of organic compounds, especially on TiO_2 colloids. [18-21] A general conclusion is that the photocatalytic reactions occur predominantly at the catalyst surface and so the specific/unspecific adsorption of ions can modify the interface properties changing the system performance [22].

The traditional approaches to study the above – mentioned adsorptive phenomena, as the study of the photodegradation kinetic, photonic efficiency [23, 24], the change in the production of active species (example reactive oxygen species, $^{\bullet}OH$, $O_2^{\bullet-}$ and H_2O_2) [25], the changes of the electrophoretic mobility of TiO_2 colloids [20, 21] and the analysis of ion partition at the solid/electrolyte interface [21], give fragmentary information about the electrical interface structure. Only a well defined characterization of this interface could give new sudden insight into the solid/electrolyte interface.

Here, we report on the study of the electrical features of the semiconductor – electrolyte interface of thin film nanocrystalline titanium dioxide electrodes in the presence of different electrolyte solutions (nature, concentration and pH). After the chemical and morphological characterization of the produced electrodes, the study of the electrical properties of the produced electrodes was carried out by electrochemical techniques (EIS and CV). Furthermore, an initial attempt of modelling of the flat band potential as a function of the chemical surface speciation was here proposed and the modelling results compared with the experimental data.

2. Experimental

2.1 Reagents and materials.

Titanium tetraisopropoxide (TIPO, purity grade 97%), butan-1-ol (99.8%), H_2SO_4 (96%), HCl (37%), Brij L4 (99%) and KCl (99.5 %) were purchased from Sigma-Aldrich, HNO_3 (65%) from Fluka, Na_2SO_4 (99%), NaOH (99%) and H_3PO_4 (85%) from Merck. All reagents were used as received, without further purification. The aqueous solutions were prepared by using water of Milli-Q purity (TOC < 2 ppb, resistivity ≥18.2 mΩ cm).

2.2 Thin film nanocrystalline TiO_2 synthesis

The thin film nanocrystalline TiO_2 electrodes were produced coating conductive glass substrates with a TiO_2 sol-gel precursor and then sintering the electrodes to obtain nanocristalline coatings. The sol-gel precursor were synthesized hydrolyzing partially a butanol solution of TIPO in nitric acid in the presence of a non-ionic surfactant (Brij L4), the obtained transparent suspension was formed by amorphous nanoparticles of TiO_2 (average diameter 2-4 nm, total loading 42 g dm^{-3} as equivalent TiO_2). The precursor were deposited as film on conductive glasses (75 × 50 × 1.1 mm, CB40INS211, Stillwater, Minnesota, USA) by dip-coating at room temperature (rate of extraction 12.5 cm×min^{-1}). After removing of the butanol for evaporation the electrodes were calcinated for 40 minutes at 550 °C in air. The conductive substrate adopted is aluminosilicate glass covered with a 150-200 nm film of Indium Tin Oxide (ITO); the declared surface conductivity of this substrate is 4 – 8 Ω □$^{-1}$. The thickness of the TiO_2 coatings were measured with a Taly Step II profilometer (Taylor Hobson): the films obtained were 80 – 100 nm thick.

2.3 TiO_2 film characterization and electrochemical experiments

The produced microfilms were characterized by using a multimodal approach. The UV-Vis spectra of the electrodes were recorded in the 250-850 nm range with a Cary 100 Scan Spectrophotometer (Varian). The refractive index in of the TiO_2 films were evaluated with a spectroscopic ellipsometer Woollam M-200 with a 75 W Xe Light Source and a Glan Taylor polarizator. The acquisition and analysis of the data were carried out with the CompleteEASE software (J. A. Woollam Co.). The film analysis were carried out between 50° and 70° of incident angle with step increment of 2.5°, acquisition time of 10 sec per step and initial alignment at 65°. The crystallographic form of the TiO_2 obtained was identified with a Horiba Jobin Yvon HR800 micro-Raman spectrometer coupled with an optical microscopy Olympus BX41. The adopted condition were: polarized argon ion laser (533 nm), 50 × optical magnification, exposition time 60 sec, hole for checking the confocality 200 μm, 633 nm Super Notch Plus to eliminate the Rayleigh scattering signal from the spectra. The re-

corded Raman spectra were the average of 4 different sequential acquisitions. The chemical composition of the produced TiO_2 film were evaluated by X-Ray Photoelectron Spectroscopy (XPS) with a Scienta ESCA 200 instrument equipped with a monochromated Al Kα source and a 200 mm hemispherical analyzer, with a pass energy of 150 eV (energy resolution 0.5 eV). The morphology of the ITO/TiO_2 electrode surfaces were evaluated with a Xe-100 PSIA atomic force microscope (AFM) in non contact modality, the 3D elaboration of the images was obtained with the XEI Version 1.1 software (PSIA). Finally, the electrochemical tests (CV and EIS) were carried out with a potentiostat galvanostat Ecochime Autolab PGSTAT12 (Utrecht, Nederland) controlled with the software GPES and FRA2 (Autolab). All the electrochemical experiments were carried out in a homemade electrochemical cell composed of a cylindrical Teflon body closed with a Pyrex glass from a side and with the working electrodes (WE) from the other side. The counter electrode (CE) was a platinum mesh (Sigma-Aldrich, 99.9%) that covers the inner wall of the cell body; the reference electrode (RE) was an external Ag/AgCl electrode (Metrohm, Swiss Confederation) filled with KCl 3M and connected to the cell with a Luggin capillary. Note that the potential of this electrode is 0.194 V vs NHE. The electrolytes were solutions of Na_2SO_4, KCl and Na_3PO_4 (ion strength = 0.3 M) at different pH for H_2SO_4, HCl, H_3PO_4 and NaOH, respectively.

3. Results and Discussion

3.1 Film characterization

The nanocrystalline titania film on conductive ITO substrate was transparent and perfectly anchored at the substrate surface. The good adhesion of the film at the substrate did not change during the electrochemical tests for all the tested electrolytes.

Figure 1 shows the UV-Vis spectrum of a TiO_2/ITO electrode compared with the transmittance % spectra of the aluminosilicate glass substrate and of the conductive ITO glass. The spectra are dominated by the absorbance in the UV region due to the band to band transitions; the shift of the

cut off to higher wavelengths (aluminosilicate glass < ITO < TiO_2) is due to the decrease of the value of the energy gap ($E_g^{aluminosilicate} > E_g^{ITO} > E_g^{TiO2}$). From the analysis of the absorbance of the TiO_2/ITO electrodes and considering that TiO_2 has an indirect band gap transition (for indirect semiconductors the optical band gap can be obtained by plotting the square root of the absorbance *vs* the energy of the photon [26]) band gap energy equal to 3.23 ± 0.08 eV was obtained. This value coincides with the band gap energy transition of the TiO_2 anatase allotrope [27]. Note that Indium Oxide is an n- type semiconductor with a direct band gap equal to 3.5–3.7 eV[28] and an indirect band gap ~ 2.6 eV [29]. The spectra of ITO glass and TiO_2/ITO electrode show different interference signals in the visible region due to the reflection of light at the interfaces between the different materials (ITO/glass, ITO/TiO_2) and the consequence constructive/destructive interference in the film layers. [30]

Raman spectroscopy is a useful tool to evaluate the crystallographic phase of titania. Rutile and anatase have well defined lattice vibrational modes in the 100-900 cm^{-1} range. Being the lattice cells of these phases highly symmetric the number of the Raman active modes is low, only six and five for anatase and rutile, respectively. [31, 32] On the contrary, the brookite lattice cell is characterized by lower symmetry than those of anatase and rutile, this has as a consequence an higher number of Raman active vibrational modes (36).[33] Figure 2 shows the Raman spectrum of the surface of a TiO_2/ITO electrode together with the position of the peaks related to the active Raman modes for anatase and rutile. The spectrum is dominated by the presence of the representative Raman peaks of anatase with no signal related to the presence of other crystalline phases.

The chemical composition of the titania film was evaluated by recording the XPS spectrum of the TiO_2/ITO electrode surface (see Figure 3). The spectrum is dominated by the XPS and Auger transition of titanium and oxygen confirming the chemical nature of the produced film. Interestingly, traces of carbon atoms were detected in the titania structure probably as a consequence of the incorporation into the TiO_2 phase of carbon atoms, originally in the organic compounds added to the sol-gel precursor (e.g. the surfactant added to increase the adhesion of the sol-gel precursor to the ITO

surface), during the calcination at 550°C. To estimate the instrumental work function it was compared the recorded position of the 1s peak of carbon with the tabulated value, the obtained value (5.6 eV) was subtracted to the energy binding of each experimental peak signal. The energy position of the main peaks recorded, their tabulated values and the nature of the correlated electronic level are reported in Table 1.

The morphology of the TiO_2/ITO electrode surface was evaluated with AFM. A 3D elaboration of a 500 nm × 500 nm surface portion is shown in Figure 4. The ITO glass was covered with a compact layer of TiO_2 formed by nanocrystalline particles with an average diameter of 30 – 60 nm. The surface roughness is extremely low and ranged in the 5-10 nm. The roughness of the conductive ITO glass surface is less than the z-axis resolution of the adopted microscopy (2 nm).

The porosity of the TiO_2 films were evaluated measuring by spectroscopic ellipsometry the refractive index of TiO_2 films in the visible. The analysis of the data was carried out considering as physical model of the TiO_2/ITO electrodes a substrate of glass covered by two different films (of ITO and TiO_2, respectively). The refractive index at 589.3 nm in the bulk of the TiO_2 film resulted equal to 2.2. By considering the refractive index of anatase equal to 2.56 **Errore. Il segnalibro non è definito.** the TiO_2 film porosity resulted equal to 14%.

3.2 Analysis of the electrochemical properties of TiO_2 electrodes

The semiconductor-electrolyte interface can be roughly divided in three different regions: the space-charge region in the semiconductor, an intermediate region called Helmholtz layer and the Diffuse Layer (DL) in solution. [34, 35] The molecules and ions in solution can give specific (or chemical) interactions with the surface or can be adsorbed with their hydration shells giving unspecific (or physical) interactions. The centre of the electric charge is placed in the former case at the so called Inner Helmholtz Plane (IHP), in the latter at the Outer Helmholtz Plane (OHP). As a consequence of the thermal movements and of the non perfect charge counterbalance between the electrode charges and the charges blocked at the Helmholtz Planes (IHP and OHP), ions and molecules of the

electrolytes diffuse near the electrode giving the Diffuse layer (DL) or Gouy – Chapman layer. Note that the formation of an important DL is a typical feature of moderately diluted electrolytes ($I < 0.1$ M), in the case of concentrated electrolytes the DL and the Helmholtz layer are not distinguished. [36] When the semiconductor/electrolyte interface is created, the Fermi levels of the semiconductor and of the solution (the redox potential, E_{redox}) equilibrate. The accumulation or depletion of minority or primary charge carriers near the semiconductor surface gives a bending of the bands which direction (anodic or cathodic) and entity depend on the *n* or *p* nature of the semiconductor and on the nature/concentration/pH of the electrolyte. Applying to the semiconductor a voltage bias is possible reinforce or deplete the band bending, the potential at which the bend bending is null is called Flat Band Potential (E_{fb}). The knowledge of this value is essential information for the characterization of the semiconductor/electrolyte interface. In a *n* semiconductor the Fermi level is located very near the conduction band, conversely in *p* semiconductor is near the valence band, so the knowledge of the E_{fb} can give the position of one of the two band and consequently of the other one knowing the Energy gap of the semiconductor. [37] Furthermore, in a photoelectrochemical cell the maximum photo-potential obtainable (E_{OCPmax}) is the different between the flat band potential and the potential of the redox couple in solution ($E_{OCPmax} = E_{fb} - E_{redox}$). [35]

Furthermore, each of the three charge structured layers formed the semiconductor/electrolyte interface can be described as a capacitor which differential capacity is defined by eq. 1

$$C = \frac{dQ}{dE} = \frac{A\varepsilon_r\varepsilon_0}{d} \qquad \text{(eq. 1)}$$

where dQ is the amount of charge blocked in the layers, dE is the relative variation of electrical potential, A is the geometric area of the two plates of the capacitor, ε_r is the dielectric constant of the dielectric, ε_0 the vacuum permittivity and d the distance between the two plates.

In the case of an ideally polarized interface the whole electrical double layers (C_{dl}) can be described as a circuit formed of three different capacitors in series, so the related total differential capacity is defined by eq. 2:

$$C^{-1} = C_{sc}^{-1} + C_{HL}^{-1} + C_{DL}^{-1} \qquad \text{(eq. 2)}$$

where C_{sc}, C_{HL} and C_{DL} are the differential capacities of the space charge layer, of the Helmholtz plane and of the Diffuse Layer, respectively. In the common semiconductor/electrolyte interfaces the distance *d* between the two plates of the ideal capacitors constituting the interface are higher for the space charge regions in comparison with those of the Helmholtz and Diffuse planes ($d_{sc} > d_{HL} \approx d_{DL}$); furthermore, the fall of potential is usually higher in the space charge than in the Helmholtz and Diffuse layers. As a consequence of this, the lower capacitance is that of the space charge layer and consequently the entire double layer differential capacitance corresponds roughly to that of the space charge layers (see eq. 2).

3.2.1 CV analysis

Cyclic voltammograms of the TiO_2/ITO electrodes were recorded in the presence of KCl, Na_2SO_4 and phosphate buffer (ionic strength = 0.3 M) at different pH (from pH 2 to 11). Note that the pHs equal to 7±1 were explored only for the phosphate buffer due to the negligible buffer power of chloride or sulfate anions. A selection of the typical patterns of CVs that were recorded with the TiO_2/ITO electrodes in the presence of the different tested electrolyte and at three different voltage scan rates is shown in Figure 5. All the CVs at acidic pH are characterized by a cathodic current follows by an anodic peak which position (peak potential, E_p, and current, i_p) is a function of the scan rate and of the electrolytes. In basic solutions the cathodic currents decrease and the anodic peak disappears (see Figure 5C). CVs of nanoporous semiconductor films have been reported widely in literature [38-40]; the recorded CVs are very similar to those reported by Fabregat-Santiago et al. [41]. These authors attributed the anodic peak to the charging and discharging of monoelectronic band gap states with an exponential band tail distribution in the energy gap. Despite of the extended states localized in the conduction band, these sites have well localized energy levels and their occupancy is a function of the potential imposed to the electrode. Figure 6 shows the shift of the peak

position (potential and current intensity) as a function of the pH for the three different electrolytes tested. The anodic peak moves toward cathodic potentials with the increment of pH; the anodic current peak decreases with the decrease of the H^+ activity in the electrolyte. The dependence of the peak potential with the pH is in all the case supernerstian with values equal to –70, –120 and –140 mV/decade for phosphate, chloride and sulfate, respectively. The peak current showed a drastic decrement of its value between pH 2 and 4, while its value was more stable at circumneutral pH.

On the basis of these experimental evidences some hypothesis on the nature of the localized states that are occupied (charged) and emptied (discharged) during the CV experiments can be done. The strong relation between the peak position and the pH suggests an active role of the acid-basic sites at the surface; these are also involved in adsorption equilibria with specific and unspecific surface interaction of ions at the surface. As example, the ligand exchange at the surface Ti(IV) sites between hydroxyl and fluoride anions is well documented [19] together with the wide changes in the photocatalytic reactivity of these fluorinated surfaces. [42-45] From this point of view the charging/discharging of the localized states can be modeled with the follow redox equilibrium

$$\equiv Ti^{(IV)}–OH + e^- + H^+ \leftrightarrows \equiv Ti^{(III)} + H_2O \qquad \text{(eq. 3)}$$

Note that the term $\equiv Ti^{(IV)}–OH$ has not a structural/crystallographic meaning, but it is intended to assemble all the Ti(IV) ions coordinated at the surface (with hydroxyl groups or water, at extended faces or in low coordination conditions [46]) and at disposal for the reported redox equilibria. The equilibrium proposed in eq. 3 explains the shift in cathodic direction of the E_p with the increment of pH and the correlated decrement of the current intensity. Furthermore, the density of $\equiv Ti^{(IV)}–OH$ groups in the protonated form and not involved in specific adsorption equilibria changes not only with the pH, but also with the nature of the Ti(IV) ligand anions in the aqueous phase. At basic pH the charge of the intraband gap states occurs at more cathodic voltages out of the potential windows that may be explored. In this condition the cathodic current is correlated with an irreversible faradic process (the reduction of H^+ to H_2). Note that in this condition a marked charge unbalancing in the cathodic direction during the CV tests was observed for all the electrolytes as a consequence of the irreversibility of the involved re-

dox couple (H^+/H_2). Conversely, in acidic condition the charge unbalancing imposed by the discharge of H^+ is compensated by the reversible nature of the charge/discharge process of the intraband gap states (see eq.3). From a circuital point of view the behavior at basic pHs can be explain considering that the faradic resistance in parallel to the space charge capacity decreases with a consequent decrement of the current through the capacitor. In this condition the charge accumulated becomes insignificant and consequently the peak in the anodic direction disappears, as modeled by Fabregat-Santiago and co-workers [41].

3.2.1 EIS results and Mott-Schottky Analysis

The use of electrochemical analytical techniques for the characterization of a system is usually based on the application of high perturbations to the electrodes (potential/current ramp or steps) that impose to the electrodes a non-equilibrium condition. An alternative approach is that of impose an alternating and small perturbation (of current or potential) and then observe the way in which the system follows the perturbations in a quasi steady state conditions. In these conditions the precision of the experiments is high because the time scale of the experiments can be higher being the system in equilibrium.[47]

The change in the electrochemical properties of the TiO_2/ITO electrodes were evaluated with this last approach by EIS in the -0.2–1 V vs Ag/AgCl voltage range as a function of the pH and of the nature of the electrolytes (KCl, Na_2SO_4 and phosphate buffer). The fit of the EIS experimental data allows us i) the identification of the best model (equivalent circuit) describing the studied electrodes; ii) the quantification of the properties of the single circuital elements. Here, we focus our attention principally to the change in the values of the electrode flat band potential and of donor density (N_d) neglecting a complete analysis of the other electric parameters for sake of brevity.

The Mott-Schottky equation correlates the capacity of the space charge layer (C_{sc}) with the imposed electrode potential E and it is applicable in the conditions in which a depletion layer is present and in the absence of faradic phenomena. In the case in which the capacity of the Helmholtz layer is

significant higher than that of the space charge layer, the Mott-Schottky equation simplify in the following form:

$$\frac{1}{C_{sc}^{\ 2}} = \left(\frac{2}{e\varepsilon\varepsilon_0 N_D}\right)\left(E - E_{fb} - \frac{kT}{e}\right) \qquad \text{(eq. 4)}$$

where e is the electron charge, N_d is the donor density, ε_r is the dielectric constant of the dielectric, ε_0 the vacuum permittivity, k the Boltzmann constant and T the temperature. From the linear fit of the Mott-Schottky plot (C_{sc}^{-2} vs E) it is possible find the flat band potential and the donor density.

All the EIS spectra, in the form of Nyquist and Bode diagrams, can be described by a $R_1(R_2C)(R_3Q)$ equivalent circuit. The physical meanings of the single circuital elements are the following.

a) R_1 is the resistance of the electrolyte solutions and of the electrical contacts. Its value is not function of the imposed potential, but varies largely with the nature of the electrolytes. From the averaged R_1 values obtained with KCl 0.1 M (specific conductivity 12.9 mS×cm^{-1}) a cell constant equal to 0.81 cm^{-1} was evaluated.

b) R_2 and C are the resistance and capacity of the electrolyte/counter electrode (CE) interface. The values of R_2 range between 0.8 and 2 Ω, while the measured capacity values are in the 35-110 μF cm^{-2} range. The electrolyte/CE capacity decreases slightly with the increment of the potential imposed to the Working electrode (WE). The values observed are reasonable for a CE formed by a Pt mesh as that used in this work.

c) R_3 is the resistance of the TiO_2/electrolyte interface. A general decrement of the R_3 values were observed at the extreme potentials as a consequence of the activation of faradic processes. The properties of the electrolyte (nature and pH) changes the R_3 values because the electric structure of the semiconductor surface/electrolyte interface changes as a consequence of the surface group speciation (dissociation degree of the acid-basic groups, adsorption phenomena). Furthermore, the R_3 values is correlated with the thickness of the TiO_2 film; a test carried out in the same conditions but with two different electrodes having film thickness equal to 220-240 nm and 80-100 nm, showed significant higher values of R_3 in the

former case (data not reported). This means that R_3 is the resistance of the entire interface and not only of the surface layers in contact with the aqueous electrolyte. Finally, the R_3 value decreases significantly if the electrode is irradiated with light able to activate band-to-band transitions ($h\nu \geq E_g$). In this case, the increment of the density of minority carriers lowers the resistance with the consequence increment of the TiO_2 film conductivity.

d) Q is the Constant Phase Element (CPE) for the TiO_2/electrolyte interface. This element is characterized by two different parameters (Y_0 and n) and the value Y_0^n can be considered approximately a capacity in particular if n is very similar to 1 and consequently the CPE showed a behavior very closed to that of an ideal capacitor [48]. For the TiO_2/ITO electrodes studied and in the voltage windows in which the Mott-Schottky plots showed linear trends (by computing the space charge capacity as Y_0^n) the n values are always in the 0.94-0.97 range.

Figure 7 shows the Mott-Schottky plots obtained with the three different electrolytes tested (KCl, Na_2SO_4 and phosphate buffer) at different pHs. The potential ranges in which the Mott-Schottky graphs showed a marked linearity are limited by the presence of an accumulation layer in the cathodic direction (at very low potentials an inversion layers can be formed) and by the starting of faradic phenomena (the water oxidation, particularly at basic pH) at high potentials. The very marked linearity ($R^2 > 0.99$) and consequently the applicability of the Mott-Schottky theory confirm that the capacitor described by the constant phase element Q is that of the space charge region which capacity changes as a function of the potential imposed to the WE (see eq. 4).

The experimental evidence that the Mott-Schottky plots of TiO_2/ITO electrodes changes as a function of the electrolyte cannot be considered an a-priori proof that the observed capacity was that of the TiO_2 coating (the more external semiconductor). In fact, it has been observed that in the case of porous TiO_2 layers (e.g. the titania film used in DSSC), the intercept of the Mott-Schottky diagrams (E_{fb}) does not change in the presence or absence of the titania layers, while changes in the slope and consequently of the donor density were observed.[49] To demonstrate that the capacity correlated with the constant phase element Q was that of the upper titania layer, two EIS experiments in the same

conditions (the same electrolyte) were carried out on the standard TiO_2/ITO electrode and on an ITO alone electrode. The results (data not reported) showed a significant variation both of the flat band potential and of the donor density, this demonstrates that the semiconductor layers observed was that of the polycrystalline TiO_2 films and confirmed the absence of porosity, as previously observed with AFM.

Figure 8 shows the change in the flat band potential and in the donor density N_d (inset of Figure 8) for the TiO_2/ITO electrodes as a function of the pH for the three different electrolytes tested.

The flat band potential decreases with the increment of pH. A linear trend in the whole pH range was observed only in the presence of the phosphate buffer, while with KCl and Na_2SO_4 a linear trend was observed only in acid condition with a an attenuated relation between E_{fb} and pH at circumneutral-basic pH. In the pH interval in which a linear relation between E_{fb} and pH was observed, slopes higher than those predicted by the Nernst equation were observed:–164, –190 and –73 mV/decade for KCl, Na_2SO_4 and phosphate buffer, respectively. For KCl and Na_2SO_4 the flattening of the relation between E_{fb} and pH happens at pH near the reported PZC for TiO_2 colloids.[19, 50] Note that limited ranges of Nernstianity of E_{fb} were also observed by Nelson and co-workers on nanoporous TiO_2 films.[20] The non-Nernstian relation between E_{fb} and pH can be rationalized (*vide infra*) on the basis of all the equilibria involving surface species (specific/unspecific adsorption, ionic exchange equilibria).

The donor density of the TiO_2 layer is reported in the inset of Figure 8 as a function of the pH in the presence of the three electrolytes tested. The N_d values, computed from the slopes of Mott-Schottky plots, vary in the 3.5-7.5×10^{-19} cm^{-3} range without marked trend with the pH. The values are in very good agreement with the N_d values reported by Gryse et al. [51] for TiO_2 electrodes reduced with H_2, while are significantly higher if compared with the values reported by Van de Krol et al. (3.5×10^{-17} and 7.9×$10^{-16}$$cm^{-3}$) for a$TiO_2$ layer after a thermal oxidative treatment (10 hours at 450°C in air). [52] The high donor density of the TiO_2/ITO electrodes studied, can be explained by considering the method of production of the nanocrystalline TiO_2 film. The high non volatile carbon

loading (non ionic surfactants) in the sol-gel precursor acts as a reducing agent during the annealing increasing the density of oxygen vacancies and in general of donor states. As commented above, the presence of residual carbon atoms in the TiO_2 lattice was observed by XPS. The absence of significant differences in the presence of different electrolytes showed that the adsorption of ions involved only surface groups without any phenomena of intercalation in the bulk TiO_2 structure.

3.2.2 Theoretical prediction of the relation between E_{fb} and pH

To better understand the role that the acid/base speciation of the OH surface groups and of the anion adsorption have on the flat band potential of TiO_2 and of semiconductors in general, we develop a semi-quantitative model for the prediction of the dependence of E_{fb} from the activity of ion H^+ in solution (a_H).

The electrochemical potentials of the H^+ ion at the surface (μ_H^{surf}) and in solution (μ_H^{sol}) are described by eq. 5 and 6.

$$\mu_H^{surf} = \mu_{H,surf}^0 + zF\Delta\phi + RT\ln x_i \qquad \text{eq. 5}$$

$$\mu_H^{sol} = \mu_{H,sol}^0 + RT\ln a_H \qquad \text{eq. 6}$$

where μ_H^{surf} and μ_H^{sol} are the electrochemical potentials of H^+ at the surface and in solution, $\mu_{H,surf}^0$ and $\mu_{H,sol}^0$ are the related standard potentials and χ_i the fraction of protonated surface groups.

At the equilibrium the two potentials assume the same value obtaining

$$zF\Delta\phi = -\Delta\mu_{transf}{}^0 + RT\ln\frac{a_H}{x_i} \qquad \text{eq. 7}$$

where $\Delta\mu_{transf}{}^0 = \mu_{H,sup}{}^0 - \mu_{H,sol}{}^0$ is the standard potential for the following equilibrium of protonation (transfer of the H^+ ion from the solution to the surface)

$$\equiv Ti^{(IV)}\text{–}OH + H^+ \leftrightarrows \equiv Ti^{(IV)}\text{–}OH_2^+ \qquad \text{eq. 8}$$

Note that the K_0 constant of this equilibrium is the inverse of the first acid dissociation constant for the acid hydroxyl groups at the surface ($K_0 = K_{a1}{}^{-1}$). The density of charge at the surface can be de-

scribed as $\sigma_s = zSFx_i$, where S is the total number of acid/base cites per unit of surface area involved in the equilibrium 8, z the charge of the exchanged ion and F the Faraday constant. To obtain a relation between the surface potential and the ion activity in solution we need a model for the studied interface with a consequent shift from a pure thermodynamic description to a structural view of the system). By considering the high ionic strength adopted for the electrochemical experiments, it is possible assume that the contribution of the diffuse layer is negligible in comparison with the capacity of the Helmholtz layer ($C_H = \frac{\sigma_s}{\Delta\phi}$) that we assume constant and equal to 90 μF cm^{-2} (ε_r = 30, d = 3 Å). By rearranging equations 7 and considering $-\Delta\mu_{trasf}{}^{0} = -RTlnK_{a1}$, one obtains the relation between the activity of H^+ in solution and the drop of potential at the surface (eq. 9).

$$a_H = \frac{K_{a1}C_H\Delta\phi}{zSF}\exp\left(\frac{\Delta\phi Fz}{RT}\right) \qquad \text{eq. 9}$$

Figure 9 (curve a) shows the relation between $\Delta\phi$ and pH as predicted by eq. 9 by using the specific values for P25 TiO_2 ($S = 2 \times 10^{-6}$ mol/m^2, pK_{a1} = 3,7) [19]. Note that the predicted drop of potential decreases linearly with a subnernstian slope equal to –53 mV/decade with a flattening near the point of zero charge (PZC). Note that subnernstian behavior of E_{fb} was reported for silicon oxide deposited on silicon with slope very closed to that predicted with our simplified model. Dort and co-workers reported for Si/SiO_2 electrode in NaCl 1M slopes equal to –50 and –46 mV/decade in the case of n-Si and p-Si, respectively [53, 54] Furthermore, the same authors reported a flattening of E_{fb} in the SiO_2 PZC region (between pH 2 and 3) [54].

To predict the role that the adsorption of a monocharged anion has on the relation E_{fb} vs pH, we introduce in the simple model above described the equilibrium reported in eq. 10 (equilibrium constant $K_{ass,x}$).

$$\equiv Ti^{(IV)}\text{–}OH_2^+ + X^- \leftrightarrows \equiv Ti^{(IV)}\text{–}X + H_2O \qquad \text{eq. 10}$$

By using competitive Langmuir adsorption equilibria and considering the electrostatic part of the equilibrium constants, the complex relation between $\Delta\phi$ and the activity of H^+ can be expressed by eq.11 (a_x is the activity in solution for the anion X^-)

$$\frac{1}{a_H} = \left[\frac{SF}{C_H \Delta\phi} - 1 - a_X K^0_{ass,x} \exp\left(\frac{-F\Delta\phi F}{RT} \right) \right] \frac{1}{K_{a1}} \exp\left(-\frac{F\Delta\phi}{RT} \right) \qquad \text{eq.11}$$

Figure 9 (curve b) shows the dependence in the case of adsorption of an anion X^- computed considering the same values adopted above and $K_{ass,x}$ = 0.01 and a_x = 0.01 M. A subnernstian slope is observed also in this case with a further decrease of the slope value (–37 mV/decade).

The experimental electrochemical data reported above showed in the case of Na_2SO_4 and KCl as electrolyte a supernernstian behavior. The two models developed failed in the prediction of this behavior. A possible drawback of the proposed model is the stability of the equilibrium constant values with pH. As we observed previously in FT-IR study of fluorinated TiO_2 surface [45], the specific adsorption of ion (in this case a strong ligand such as the anion F^-) modifies the Lewis acidity of Ti(IV) sites with an increment of the hydrophilicity of the surface. Supposing that the K_{a1} value changes with the pH decreasing from 5.7 to 3.7 from pH 2 and pH 4, a supernernstian behavior of the E_{fb} is predicted as show in the inset of Figure 9 (slope –95 mV/decade).

In the presence of phosphate buffer as electrolytes the significant change in the relation between E_{fb} and pH can be explained considering that phosphate ion adsorbed strongly at the surface [20] modifying the nature of the surface groups and consequently the speciation of the hydroxyl groups at the surface.

4. Conclusions

The relation between the nature of the adopted aqueous electrolyte and the electrical properties of nanocrystalline thin film TiO_2 electrodes were investigated by CV and EIS.

The CV tests emphasized that the activity and the nature of the ions in solution can affect the density of monoelectronic band gap states (with an exponential band tail distribution in the semicon-

ductor energy gap) which degree of occupancy can change not only as a function of the potential imposed to the WE, but also to the chemical speciation of the surface groups.

The study by EIS of the TiO_2/ITO electrodes emphasized a non nernstian behaviour of the flat band potential (E_{fb}) as a function of the electrolytes solutions. This is in contrast with the data usually reported in literature [20, 55, 56] and shows that not only the H^+ and OH^- ions but also other ions could be Potential Determining Ions (PDI) for nanocrystalline titanium dioxide electrodes. These conclusions, supported by the preliminary modelling data here showed, are significant for a complete electrical characterization (position of the valence and conduction band, width of the space charge region, presence of surface states…) of the titanium dioxide – electrolyte interface.

The behaviour of the E_{fb} and, as a consequence, of the surface charge of the semiconductor is controlled by the specific adsorption of ions. In turn, if the ions do not charge completely the surface, the specific adsorption can induce variation in the acid/base properties of the residual hydroxyl groups. In this case a simple model which considers the surface pKa of OH groups constant fails to describe the system and could be the reason of the observed supernernstian behaviour of E_{fb}. These effects can allow a fine tuning of band edge position and are of interest for several applications of photoeffects on semiconductor oxides (photocatalysis, DSSC, H_2 generation). Further experimental and theoretical work is ongoing to unravel this complex picture.

Acknowledgment. Financial support by EU Commission – Project SETNanoMetro No. 604577 (FP7-NMP-2013-LARGE 7) is gratefully acknowledged. MM is thankful to Rockwood Italia S.p.A. Divisione Silo for the economic support to his research activity.

Table 1 Main peaks observed in the XPS spectrum of the TiO_2/ITO electrode surface: experimental energy of the detected peaks, tabulated values and corresponding electronic levels. [57]

Electronic Level	*Measured energy, eV*	*Tabulated energy, eV*
Ti 3p	37.5	37.4
Ti 3s	62.0	63.0
C 1s	285.0	285.0
Ti 2p 3/2	459.0	458.6
Ti 2p 1/2	464.5	464.6
O 1s	530.0	529.4
Ti 2s	565.5	565.3
O KL23L23	974.5	976
O KL1L23	995.5	997
Ti KL1L1	1072.5	1072
Ti LMM	1106.0	1106
C KL23L23	1225.5	1226

Captions to the Figures

Figure 1 UV-Vis transmittance spectra of the *i)* aluminosilicate glass substrate; *ii)* Indium Tin Oxide conductive glass and *iii)* TiO_2/ITO electrode.

Figure 2 Raman spectrum of the TiO_2 nanocrystalline film deposited over the conductive glass substrate. The vertical solid lines show the typical Raman peak signals of anatase, the vertical dotted lines those of rutile. **Errore. Il segnalibro non è definito.**, **Errore. Il segnalibro non è definito.**

Figure 3 XPS spectra of the TiO_2/ITO electrode in the 0 – 1486 eV range. The identification of the main XPS and Auger peaks is reported in figure.

Figure 4 500 nm × 500 nm Atomic Force Microscopy image of the TiO_2/ITO electrode surface.

Figure 5 CVs of ITO/TiO_2 electrodes at three different voltage scan rates (0.2, 0.1 and 0.05 V s^{-1}) in the presence of KCl (ionic strength 0.3 M) at three different pH: A) 2; B) 4 and C) 10.8.

Figure 6 Position of the anodic peak (A: potential; B: current intensity) recorded in the cyclic voltammograms of ITO/TiO_2 electrodes in the presence of KCl, Na_2SO_4 or phosphate buffer at different pH (ionic strength 0.3 M).

Figure 7 Mott-Schotty plots for the TiO_2/ITO electrodes at different pH in the presence of different electrolytes (I = 0.3 M): A) KCl; B) Na_2SO_4; C) phosphate buffer.

Figure 8 Formal flat band potential (E_{fb}) and donor density (N_d, inset) as a function of the pH in the presence of different electrolytes (KCl, Na_2SO_4 and phosphate buffer).

Figure 9 Surface potential as a function of the pH as predicted by a model with a constant capacity for the Helmholtz layer and that considers (a) only the first acid dissociation for hydroxyl groups of TiO_2 surface, (b) the first acid dissociation and an equilibrium of adsorption of a generic anion monocharged. Inset: Surface potential predicted as in (a) but with three different pK_{a1} values.

Figure 1

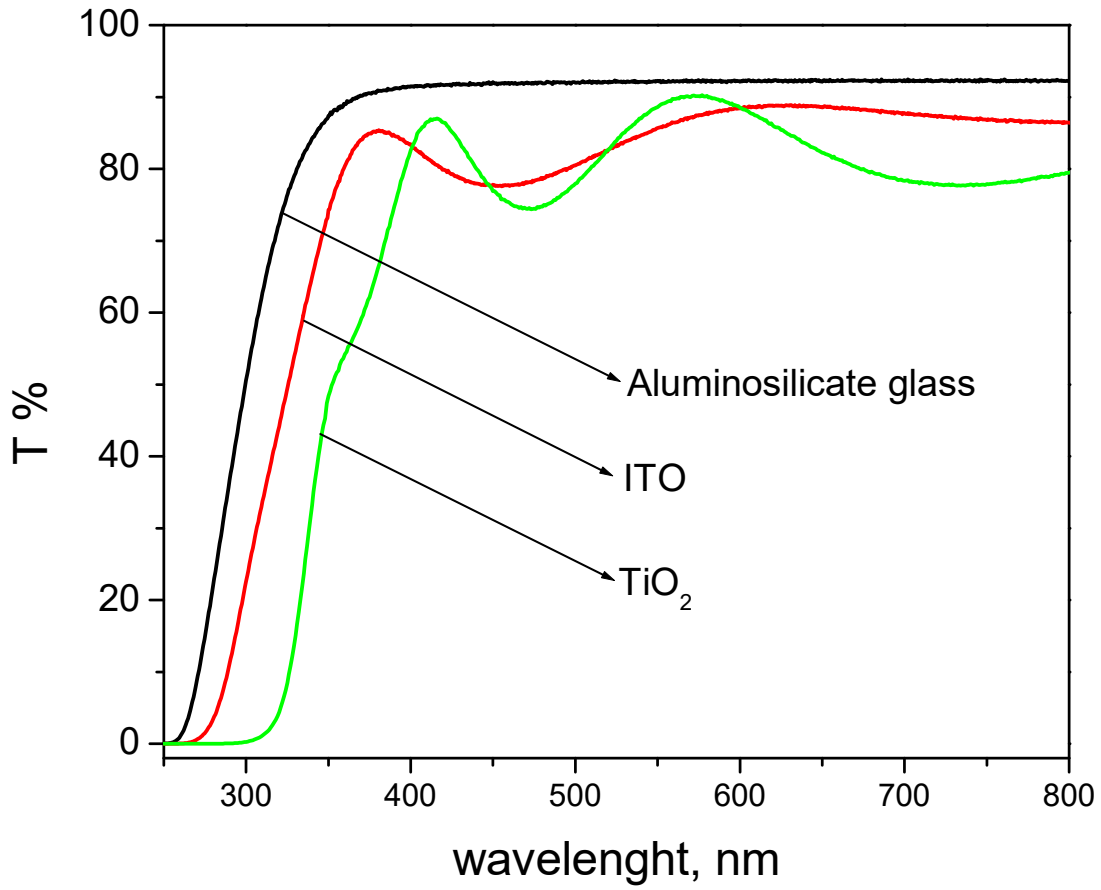
100
80
60
40
20
0
T %
300
400
500
600
700
800
wavelenght, nm
Aluminosilicate glass
ITO
TiO2

Figure 2

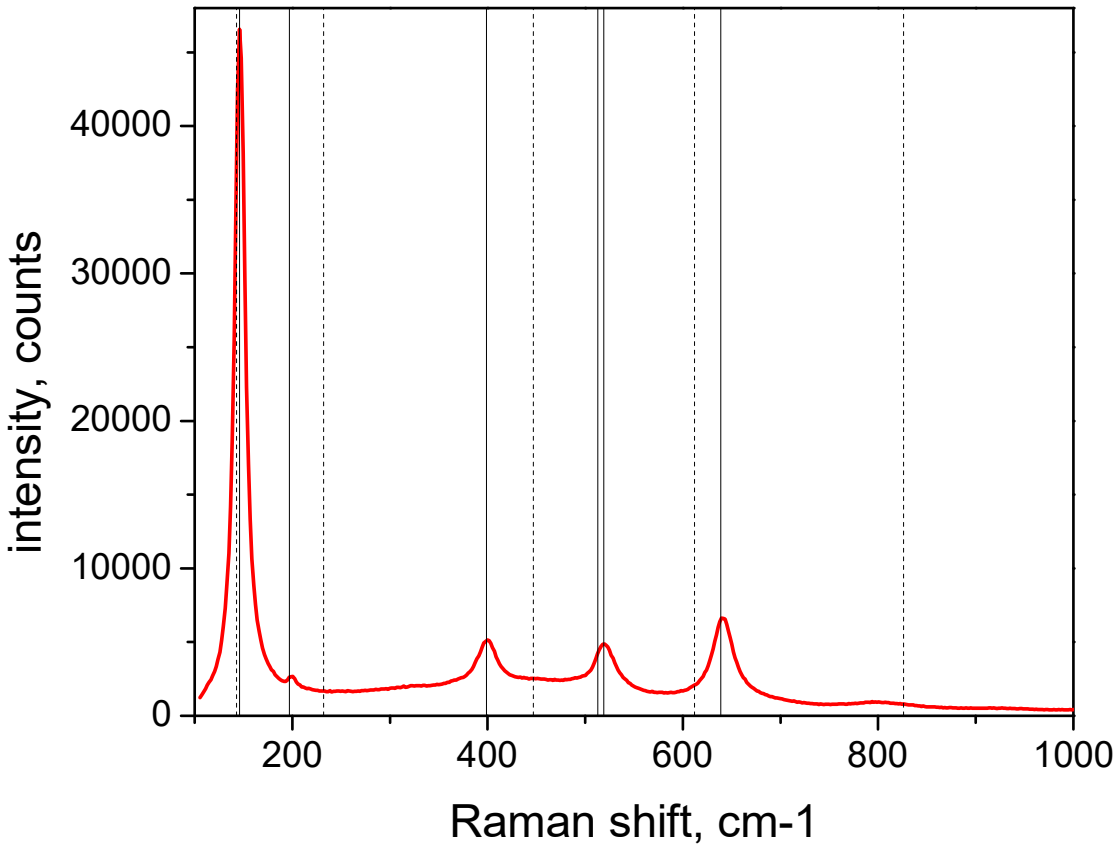
intensity, counts
40000
30000
20000
10000
0
200
400
600
800
1000
Raman shift, cm-1

Figure 3

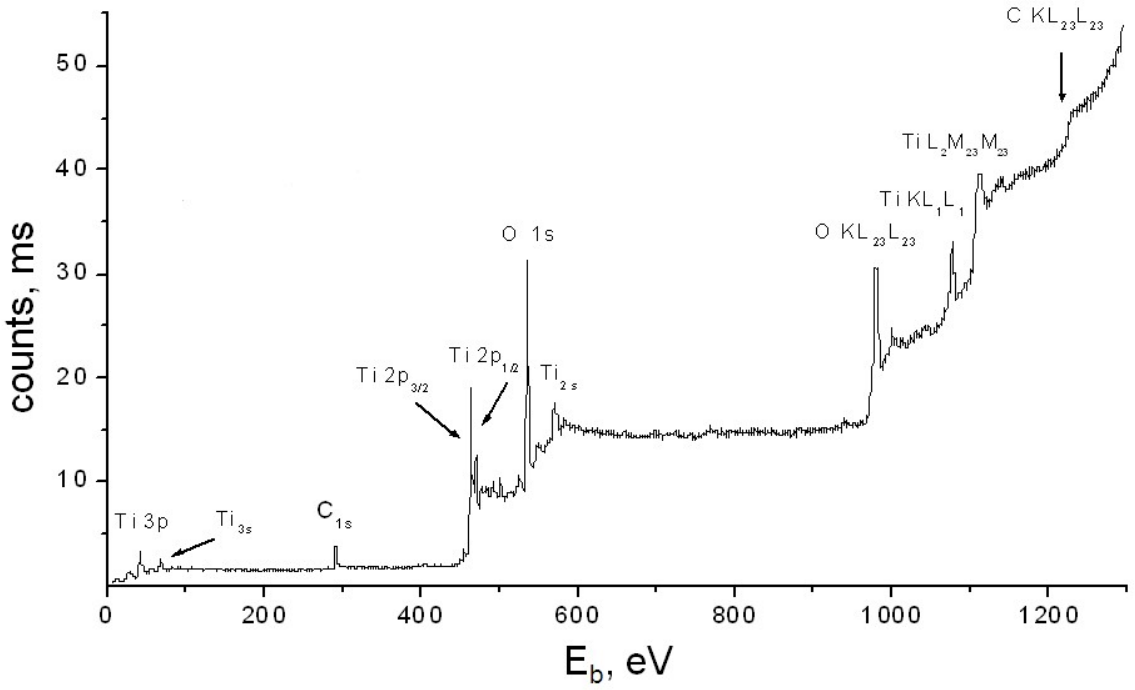
C KL23L23
Ti L2M23M23
Ti KL1L1
O KL23L23
O 1s
Ti 2p1/2
Ti 2p3/2
Ti2s
Ti 3p
Ti3s
C1s
counts, ms
Eb, eV
0
200
400
600
800
1000
1200
10
20
30
40
50

Figure 4

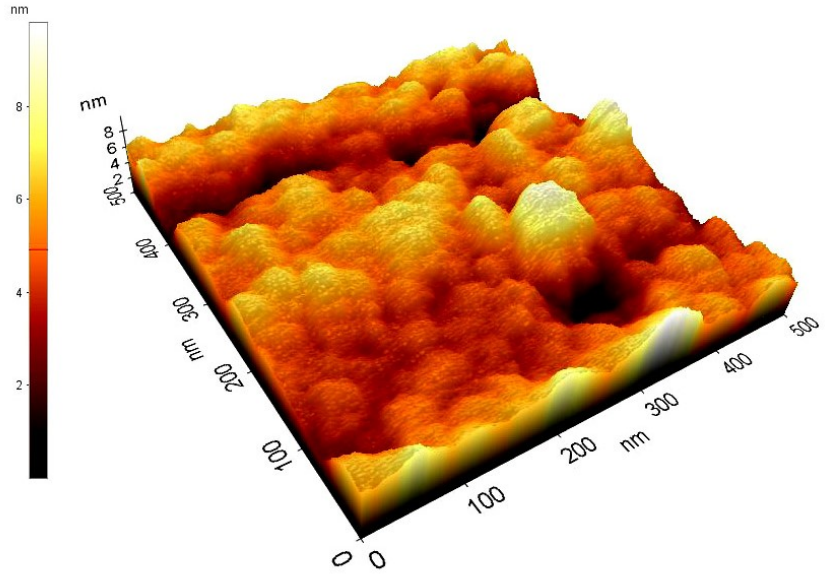

Figure 5

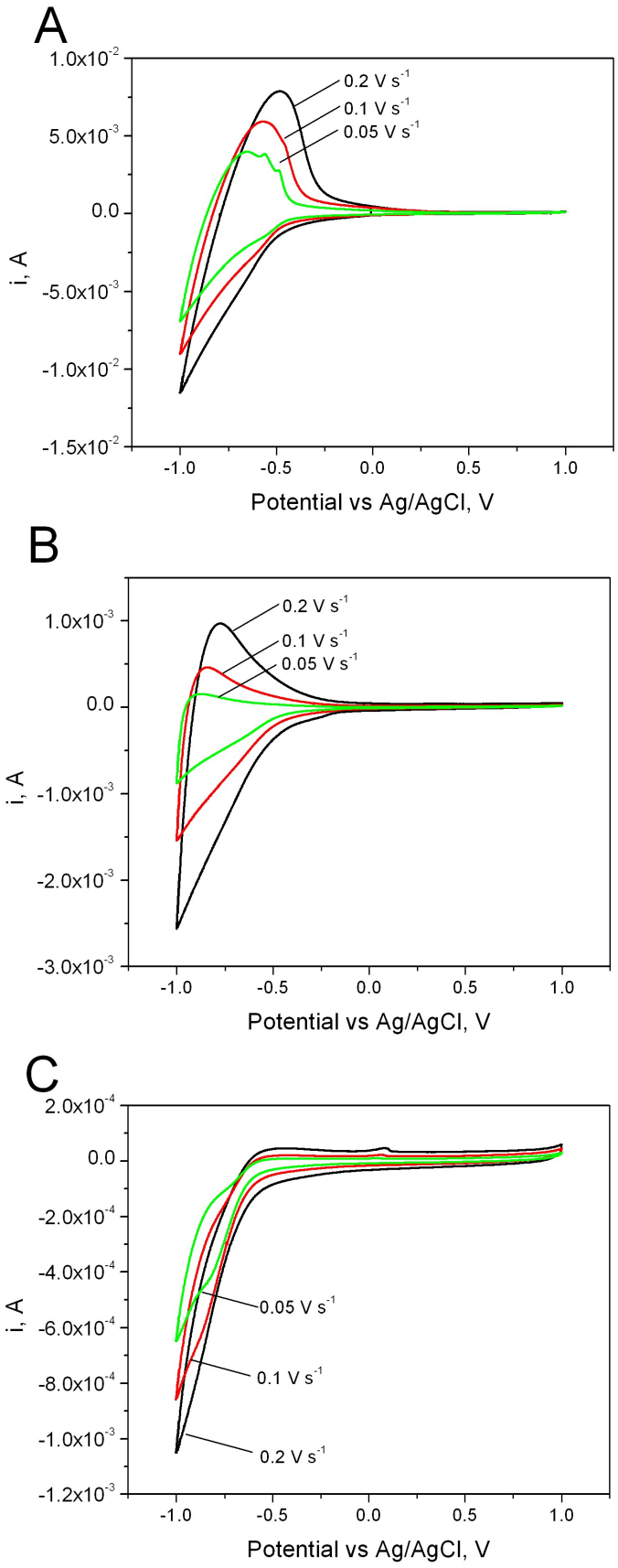
A
1.0x10-2
5.0x10-3
0.0
-5.0x10-3
-1.0x10-2
-1.5x10-2
i, A
0.2 V s-1
0.1 V s-1
0.05 V s-1
-1.0
-0.5
0.0
0.5
1.0
Potential vs Ag/AgCl, V
B
1.0x10-3
0.0
-1.0x10-3
-2.0x10-3
-3.0x10-3
i, A
0.2 V s-1
0.1 V s-1
0.05 V s-1
-1.0
-0.5
0.0
0.5
1.0
Potential vs Ag/AgCl, V
C
2.0x10-4
0.0
-2.0x10-4
-4.0x10-4
-6.0x10-4
-8.0x10-4
-1.0x10-3
-1.2x10-3
i, A
0.05 V s-1
0.1 V s-1
0.2 V s-1
-1.0
-0.5
0.0
0.5
1.0
Potential vs Ag/AgCl, V

Figure 6

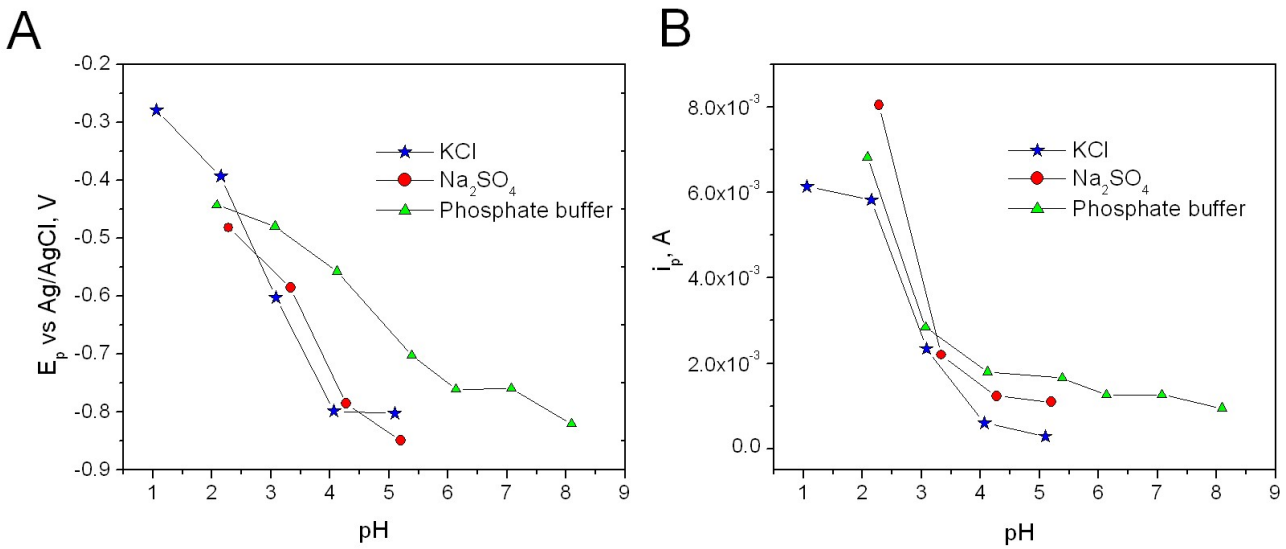

Figure 7

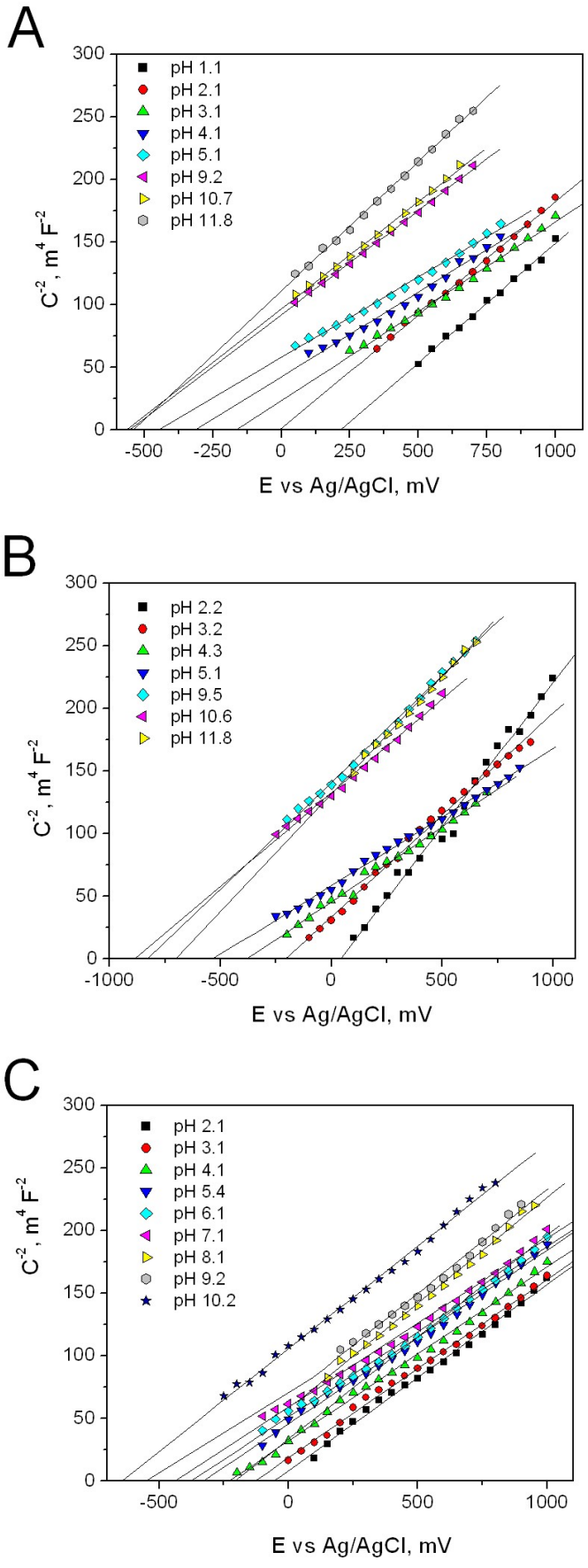
A
pH 1.1
pH 2.1
pH 3.1
pH 4.1
pH 5.1
pH 9.2
pH 10.7
pH 11.8
C-2, m4 F-2
E vs Ag/AgCl, mV
B
pH 2.2
pH 3.2
pH 4.3
pH 5.1
pH 9.5
pH 10.6
pH 11.8
C-2, m4 F-2
E vs Ag/AgCl, mV
C
pH 2.1
pH 3.1
pH 4.1
pH 5.4
pH 6.1
pH 7.1
pH 8.1
pH 9.2
pH 10.2
C-2, m4 F-2
E vs Ag/AgCl, mV

Figure 8

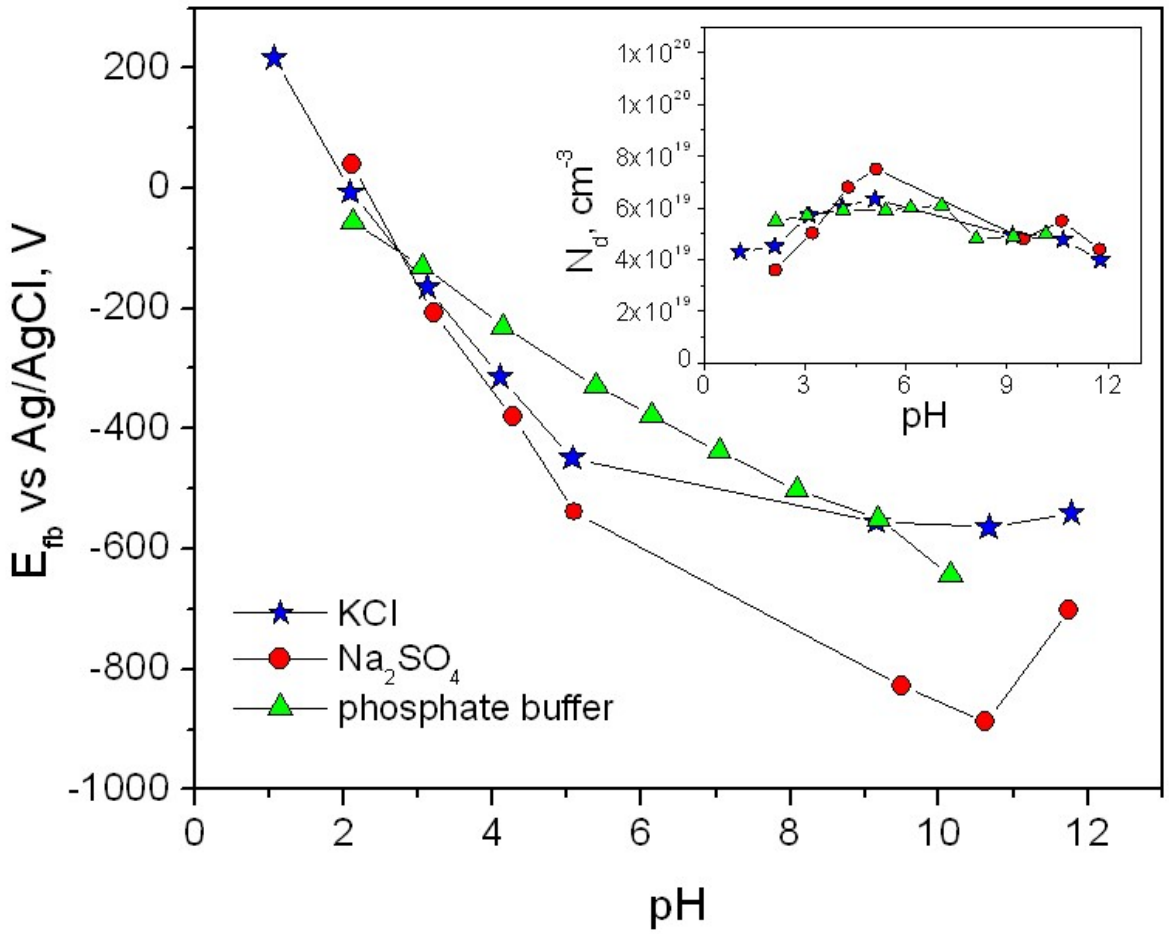
200
0
-200
-400
-600
-800
-1000
0
2
4
6
8
10
12
pH
E_fb vs Ag/AgCl, V
KCl
Na2SO4
phosphate buffer
1x10^20
1x10^20
8x10^19
6x10^19
4x10^19
2x10^19
0
N_d', cm^-3
0
3
6
9
12
pH

Figure 9

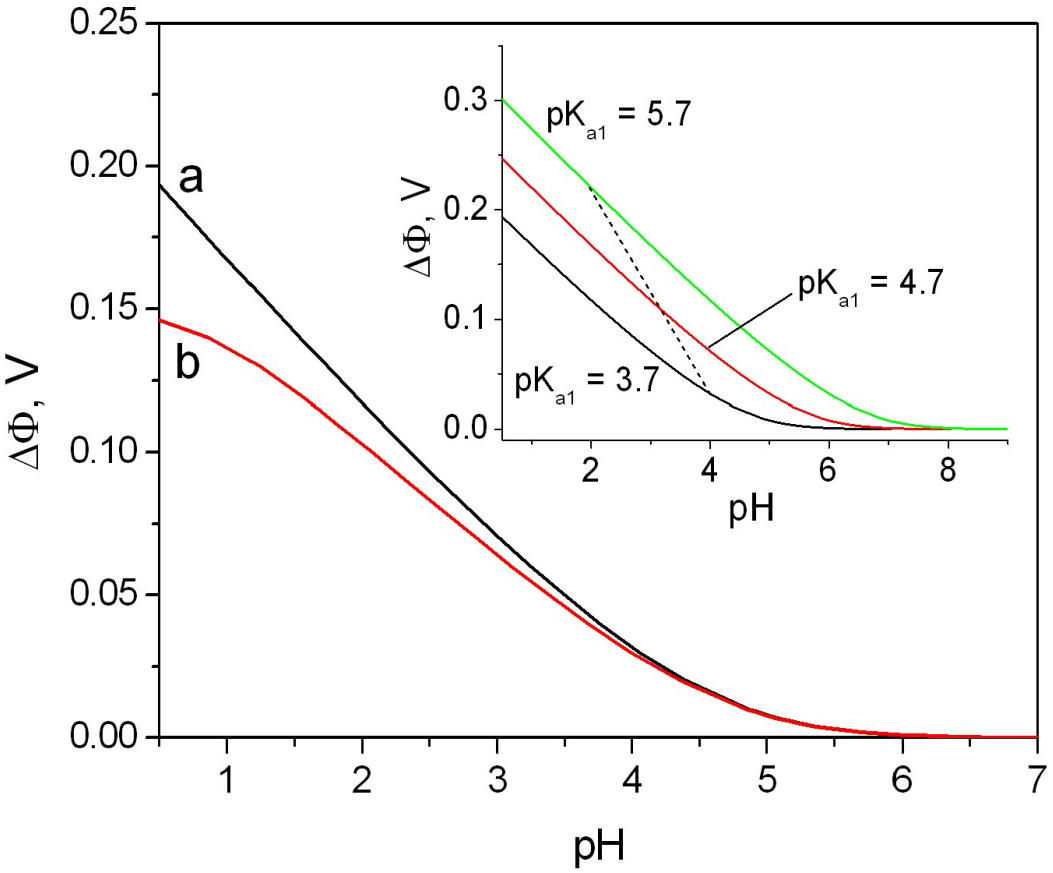
0.25
0.20
0.15
0.10
0.05
0.00
ΔΦ, V
a
b
1
2
3
4
5
6
7
pH
0.3
0.2
0.1
0.0
ΔΦ, V
pK$_{a1}$ = 5.7
pK$_{a1}$ = 4.7
pK$_{a1}$ = 3.7
2
4
6
8
pH

References

1. T. N. Obee and R. T. Brown, Environ. Sci. Technol. 29, 1223 (1995)
2. N. J. Lawryk and C. P. Wiesel, Environ. Sci. Technol. 30, 810 (1996)
3. K. Li, S. Y. C. Liu, C. Huang, S. Esariyaumpai and D. H. Chen, J. Adv. Oxid. Technol. 5, 227 (2002)
4. H. Chen, C. E. Nanayakkara and V. H. Grassian, Chem. Rev. 112, 5919 (2012)
5. A. Fujishima, T. N. Rao and D. A. Tryk, J. Photochem. Photobiol. C-Photochem. Rev. 1, 1 (2000)
6. D. Fabbri, A. Bianco Prevot and E. Pramauro, J. Appl. Electrochem. 35, 815 (2005)
7. D. Vione, C. Minero, V. Maurino, M. E. Carlotti, T. Picatonotto and E. Pelizzetti, Appl. Catal. B-Environ. 58, 79 (2005)
8. L. L. Lifongo, D. J. Bowden and P. Brimblecombe, Chemosphere 55, 467 (2004)
9. V. Maurino, C. Minero, E. Pelizzetti and M. Vincenti, Colloid Surf. A-Physicochem. Eng. Asp. 151, 329 (1999)
10. J. L. Wang and L. J. Xu, Crit. Rev. Environ. Sci. Technol., 42, 251 (2012)
11. S. Ahmed, M.G. Rasul, W. N. Martens, R. Brown and M.A. Hashib, Desalination 261, 3 (2010) 261
12. R. Wang, K. Hashimoto and A. Fujishima, Nature 388, 431 (1997)
13. A. V. Emeline, A. V. Rudakova, M. Sakai, T. Murakami and A. Fujishima, J. Phys. Chem. C 117, 12086 (2013)
14. B. E. Hardin,H. J. Snaith, M. D. McGehee, Nat. Photonics 6, 162 (2012)
15. B. O'Regan and M. Grätzel, Nature 353, 737 (1991)
16. Q. Wang, J. E. Moser and M. Grätzel, J. Phys. Chem. B 109, 14945 (2005)
17. D. Wei, Int. J. Mol. Sci. 11, 1103 (2010)
18. P. Calza and E. Pelizzetti, Pure Appl. Chem. 73, 1839 (2001)
19. C. Minero, G. Mariella; V. Maurino and E. Pelizzetti, Langmuir 16, 2632 (2000)
20. B. P. Nelson, R. Candal, R. M. Corn and M. A. Anderson; Langmuir 16, 6094 (2000)
21. V. Maurino, C. Minero, E. Pelizzetti, G. Mariella, A. Arbezzano and F. Rubertelli, Res. Chem. Intermed. 33, 319 (2007)
22. C. Minero, F. Catozzo and E. Pelizzetti, Langmuir 8, 481 (1992)
23. C. H. Hsiao, C. L. Lee and D. F. Ollis, J. Catal. 82, 418 (1983)
24. S. T. Martin, H. Hermann and M. R. Hoffmann, J. Chem. Soc. Faraday Trans. 90, 3323 (1994)
25. V. Maurino, C. Minero, G. Mariella and E. Pelizzetti, Chem. Commun. 20, 2627 (2005)
26. E. Rosencher and B. Vinter, *Optoelectronics*, Cambridge University Press, Cambridge (2002)
27. U. Diebold, Surf. Sci. Rep. 48, 53 (2003)
28. D. Liu, W. W. Lei, B. Zou, S. D. Yu, J. Hao, K. Wang, B. B. Liu, Q. L. Cui and G. T. Zou, J. Appl. Phys. 104, 083506 (2008)
29. R. L. Weiher and R. P. Ley, J. Appl. Phys. 37, 299 (1966)
30. H. Fujiwara, *Spectroscopic Ellipsometry: Principles and applications*, John Wiley & Sons, New York (2007)
31. V. Swamy, A. Kutznetsov, L.S. Dubrovnsky, R.A. Caruso, D.G. Shchukin and B.C. Muddle, Phys. Rev. B 71, 184302 (2005)
32. T. Lu, L. Lin, X. Zu, S. Zhu and L. Wang, Nucl. Instr. and Meth. in Phys. Res. B 218, 111 (2004)
33. G.A. Tompsett, G.A. Bowmaker, R.P. Cooney, J.B. Metson, K.A. Rodgers, J.M. Seakins, J. Raman Spectrosc. 26, 57 (2005)
34. J. O'M. Bockris and A. K. N. Reddy, *Modern Electrochemistry Volume 2*, Plenum / Rosetta Edition, New York (1970)
35. A. J. Nozik and R. Memming, J. Phys. Chem. 100, 13061 (1996)

36. Y. V. Pleskov and Y. Y. Gurevich, *Semiconductor photoelectrochemistry*, Consultants Bureau, New York (1986)
37. M. Grätzel, Nature 414, 338 (2001)
38. L.A. Lyon and J.T. Hupp; J. Phys. Chem. B 103, 4623 (1999)
39. E. Meulenkamp, J. Phys. Chem. B 103, 7831 (1999)
40. P. Hoyer and H. Weller, J. Phys. Chem. 99, 14995 (1995)
41. F. Fabregat-Santiago, I. Mora-Serò, G. Garcia-Belmonte and J. Bisquert, J. Phys. Chem. B 107, 758 (2003)
42. C. Minero, G. Mariella, V. Maurino, D. Vione and E. Pelizzetti, Langmuir 16, 8964 (2000)
43. H. Park and W. Choi, J. Phys. Chem. B 108, 4086 (2004)
44. M. Mrowetz and E. Selli, Phys. Chem. Chem. Phys. 7, 1100 (2005)
45. M. Minella, M. G. Faga, V. Maurino, C. Minero, E. Pelizzetti, S. Coluccia and G. Martra, Langmuir 26, 2521 (2010)
46. C. Deiana, M. Minella, G. Tabacchi, V. Maurino, E. Fois and G. Martra, Phys. Chem. Chem. Phys., 15, 307 (2013)
47. A. J. Bard and L. R. Faulkner, *Electrochemical Method Foundamentals and Applications*, John Wiley & Sons, New York (1980)
48. E. Barsoukov and J. R. Macdonald, *Impedance Spectroscopy Theory, Experiment, and Application*, second edition, Wiley – Interscience, Hoboken (2005)
49. F. Fabregat-Santiago, G. Garcia-Belmonte, J. Bisquert, P. Bogdanoff and A. Zaban, J. Electrochem. Soc. 150, 293 (2003)
50. D. Vasudevan, A. T. Stone, Environ. Sci. Technol. 30, 1604 (1996)
51. R. De Gryse, W. P. Gomes, F. Cardon and J. Vennik, J. Electrochem. Soc. 122, 711 (1975)
52. R. van de Krol, A. Goossens and J. Schoonman, J. Electrochem. Soc. 144, 1723 (1997)
53. J. L. Dort, J. Joseph, J. R. Martin, and P. Clechet, J. Electroanal. Chem. 193, 75 (1985)
54. X. G. Zhang, *Electrochemistry of Silicon and Its Oxide*, Kluwer Academic Publishers, New York (2004)
55. M. Grätzel, in *Photocatalysis: Fundamentals and Applications* edited E. Pelizzetti and N. Serpone, Wiley Interscience, New York (1989), p. 123
56. M. D. Ward, J. R. White and A. J. Bard, J. Am. Chem. Soc. 105, 27 (1983)
57. Alexander V. Naumkin, Anna Kraut-Vass, Stephen W. Gaarenstroom and Cedric J. Powell, NIST X-ray Photoelectron Spectroscopy Database, NIST Standard Reference Database 20, Version 4.1 (2012)

Colored Graphical Abstract

Thin film nanocrystalline TiO_2 electrodes: dependence of flat band potential on pH and anion adsorption

M. Minella, V. Maurino, C. Minero, E. Pelizzetti

A multimodal analytical approach was used for a complete characterization of nanocrystalline TiO_2 electrodes together with their electrochemical properties. Particular attention was devoted to the relation between the semiconductor flat band potential and the adopted electrolyte.